J|A|C|S COMMUNICATIONS

Published on Web 02/16/2010

Fabrication of Ag@SiO_2@Y_2O_3:Er Nanostructures for Bioimaging: Tuning of the Upconversion Fluorescence with Silver Nanoparticles

Fan Zhang,[†,‡] Gary B. Braun,[†] Yifeng Shi,[†] Yichi Zhang,[†] Xiaohong Sun,[†] Norbert O. Reich,[†] Dongyuan Zhao,[‡] and Galen Stucky*[,†]

Department of Chemistry and Biochemistry, University of California, Santa Barbara, California 93106, and Department of Chemistry and Laboratory of Advanced Materials, Fudan University, Shanghai 200433, P. R. China

Received October 26, 2009; E-mail: stucky@chem.ucsb.edu

The optical properties of a photoluminescence (PL) material positioned in close proximity to colloidal metal nanoparticles are affected by the near-field electrodynamical environment.[1] The modified fields cause an enhancement or quenching of the PL relative to the native state, which depends sensitively on the distance between the material and the metal surface. Recently, a number of interesting systems of nanostructures of metal cores, spacer molecules, and PL materials have been examined.[1−3] The distance dependency of PL enhancement and quenching have so far been observed with organic dyes,[1] quantum dots,[2] and rare-earth (RE) complexes[3] with organic molecules,[3] polyelectrolytes,[1] or silica[2] as spacers. Potential applications of metal-induced PL enhancement/quenching range from sensing technologies[4] to solid-state lighting.[5]

Among the many types of PL nanoparticles, upconversion (UC) nanomaterials have several advantages over the conventional organic dye markers and quantum dots,[6] including high chemical stability, low toxicity, and a high signal-to-noise ratio.[6] Recently, the coupling of RE ions with metal nanomaterials has been developed as a valuable strategy to enhance the luminescence of RE ions.[7,8] Until now, metal-enhanced UC fluorescence efforts have focused on glass composites[7] and films.[8] However, there have been no reports on the fabrication of uniform and dispersed UC nanoparticles exploiting metal enhancement, which could increase the PL performance in biological and nanophotoelectronic applications.

In the present work, we report a facile method to fabricate metal core enhanced Er materials based on a core/spacer/shell approach. We systematically increase the spacer thickness to optimize Ag@SiO_2@Y_2O_3:Er nanostructure materials. Tuning by switching between UC fluorescence enhancements and quenching is shown to be dependent on the dielectric silica spacer thickness, a parameter easily controlled during synthesis.

The procedure for creating a Ag@SiO_2@Y_2O_3:Er nanostructure is illustrated in Figure 1a. First, water-soluble silver nanoparticles (AgNPs) were synthesized in the presence of polyvinylpyrrolidone by heating ethylene glycol and $AgNO_3$ (Figure S1).[9] Through a modified Stöber method,[10] the AgNPs were coated with a silica layer to obtain a Ag@SiO_2 composite. Using ∼50 nm AgNPs, the resulting Ag-50*nm*@SiO_2 spheres have a uniform diameter of ∼190 nm and contain one ∼50 nm AgNP each, positioned at the center (Figure 1b). The SiO_2 thickness can be controlled by changing the reaction time and silica precursor concentration. The uniform Ag@SiO_2 spheres were then coated with a layer of Y, $Er(OH)CO_3 \cdot H_2O$ through a homogeneous precipitation method from yttrium, erbium nitrate, and urea at 90 °C for 2 h.[11] After heat treatment at 700 °C for 3 h, the amorphous Y:$Er(OH)CO_3 \cdot H_2O$ layer transforms into cubic phase Y_2O_3:Er (spacegroup *Ia*3 (206))

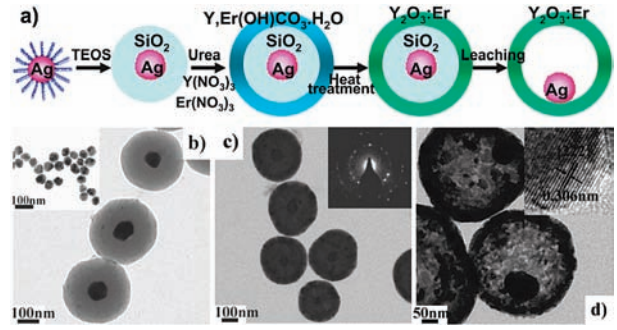

Figure 1. (a) Synthetic procedure of the Ag@SiO_2@Y_2O_3:Er nanostructures. TEM images of (b) Ag-*50nm*@SiO_2 nanospheres, with inset showing Ag NPs with 50 nm diameter; (c) Ag-*50nm*@SiO_2@Y_2O_3:Er nanospheres, with inset showing SAED patterns recorded on the Y_2O_3:Er layer (inset is higher magnification image of a single nanosphere); (d) Ag-*50nm*@Y_2O_3:Er hollow nanospheres, with inset showing HRTEM of the Y_2O_3:Er layer.

with lattice constant $a = 1.05$ nm (Figures 1c and S2). The thickness of this layer in the Ag@SiO_2@Y_2O_3:Er nanostructure is ∼20 nm (Figure 1c). SAED patterns recorded from the Y_2O_3:Er layer confirm a polycrystalline feature (Figure 1c inset).[10] An HRTEM image of the Y_2O_3 layer reveals a distance of 0.306 nm of the crystal fringes, which is assigned to the {222} crystal plane of the Y_2O_3 bcc phase (Figure 1d inset). Finally, silica leaching generates hollow Ag@Y_2O_3:Er nanospheres (Figure 1d). Ag cores with diameters from 20 to 130 nm were used to synthesize a series of the Ag@Y_2O_3:Er core/shell hollow nanospheres (Figure S3).

The UV−vis−NIR spectrum of the Ag NPs shows the well-known surface plasmon resonance (SPR) band at 380−420 nm of nanosized Ag (Figure S4a, Table S1).[12] The SPR peak shifts toward a longer wavelength as the silica shell is grown due to the local refractive index change around the particles (Figure S4b). Ag-free Y_2O_3:2% Er hollow nanospheres have seven sharp absorption bands due to 4*f* intrashell transitions arising from the ground state $^4I_{15/2}$ of Er^{3+} (Figure S4f), whereby Ag@SiO_2@Y_2O_3:Er displays a broadened absorption band in addition to the small peaks inherent to Er^{3+} (Figure S4c−d).

Upconversion emission spectra of Y_2O_3:2% Er hollow nanospheres obtained at 980 nm excitation (Figure 2Ab) reveals a weak band at 525 nm and two prominent upconverted peaks at 550 and 660 nm, which can be assigned to the (i) $^2H_{11/2} \rightarrow {}^4I_{15/2}$, (ii) $^4S_{3/2} \rightarrow {}^4I_{15/2}$, and (iii) $^4F_{9/2} \rightarrow {}^4I_{15/2}$ transitions, respectively (Figures S5,6).[12] Silica-spaced nanostructures (Figure 2Aa,c,e with 30, 70, and 0 nm SiO_2) reveal that the emission intensity is sensitive to the distance between the AgNP and Y_2O_3:Er shell. We obtained PL enhancement factors in Figure 2B by dividing integrated PL intensities of the samples with AgNPs (Figure 2Aa,c,e) by those without (Figure 2Ab).

[†] University of California.
[‡] Fudan University.

10.1021/ja909108x

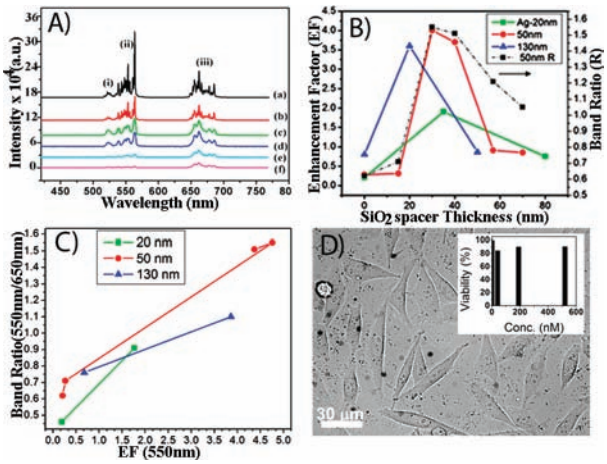

Figure 2. Upconversion spectra of *Ag-core@SiO$_2$-spacer@*20 nm-Y_2O_3 depends on spacer thickness. (A) (a) Ag-*50nm*@SiO_2-*30nm*@Y_2O_3:Er, (b) No Ag, Y_2O_3:Er, (c) Ag-*50nm*@SiO_2-*70nm*@Y_2O_3:Er, (d) Ag-*130nm*@Y_2O_3:Er, (e) Ag-*50nm*@Y_2O_3:Er, and (f) Ag-*20nm*@Y_2O_3:Er. (B) Enhancement factors (EF) averaged between 550 and 650 nm for the three Ag sizes, and (black trace) normalized integrated green to red intensity ratio (Band Ratio) for Ag-*50nm*@SiO_2-*30nm*@Y_2O_3:Er as a function of the SiO_2 spacer thickness. (C) Band ratio versus EF at 550 nm for the three Ag cores/spacers with an EF less than or equal to the maximum. (D) Prostate cancer cell imaging after overnight incubation with particles and MTS viability graph as inset.

Figure 2B reveals that, with a thin SiO_2 spacer, the PL is quenched (Enhancement factors (EF) < 1). We attribute this to the close proximity of the Ag sphere with the shell causing efficient nonradiative energy transfer from the luminescent system to the metallic surface, consistent with recent reports.[1−3] Interestingly, the fluorescence intensity of the zero-spacer Ag-130*nm*@Y_2O_3:Er is only slightly quenched which may result from the greater scattering enhancement of the large AgNP.[13]

With increasing spacer thickness the average PL intensity reaches a maximum value of 4× that from the pure Y_2O_3:Er shell at an optimal spacer thickness of 30 nm (Figure 2B,C). This enhancement factor reverts to approximately unity for larger spacer thicknesses as expected (Figure 2B and Table S1). Generally we observed larger EF for the 550 nm band, as the plasmon has better overlap. The significant fluorescence enhancement from Ag-*50nm*@SiO_2-*30nm*@Y_2O_3:Er RE ions indicates that quenching is competitive but weaker than enhancement, especially at and beyond an ∼30 nm spacer distance. This enhancement is attributed to the greater emission rate of the RE ions, caused by the strong Ag plasmon resonance scattering.[1−3,8,9] Since the Ag plasmon has a weak absorbance at the excitation wavelength (980 nm), we expect the absorbance rate of the Y_2O_3:Er nanostructures to be unmodified. The PL decays of Ag-core particles were shorter than those of reference particles without a metal core, which is in accordance with previously described metal-enhanced fluorescence (MEF) (Table S1 and Figure S7).[1−3]

We also found that the ratio of the band ($R = I_g/I_r$) tracks the EF across the range of SiO_2 spacers, demonstrating a preferential enhancement of the green emission band. Figure 2C shows that as the nanostructure EF at 550 nm increases, the material's R value is different. We can rationalize these properties in terms of a wavelength- and distance-dependent enhancing/quenching for the three cores wherein the enhancing component comes from a scattering cross section (Sca) and a quenching due to the nonradiating plasmon absorbance (Abs). These quantities are expected to be dependent on AgNP size (Figure S8).[13] Small Ag only weakly scatters and has the most narrow resonance near 400 nm, therefore having a low Sca/Abs value, and prefers quenching the green RE emission (Figure 2B−C, green). In contrast, 130 nm Ag should have a relatively high Sca/Abs with a broader profile (especially for nonspherical particles),[13] scattering more equally across the green and red portions[13] so that $R \approx 1$. The most promising material in this study, the 50 nm Ag, is between these regimes with a significant band ratio of ∼1.6 and the largest EF (Figure 2B−C, red). The 50 nm Ag@Y_2O_3:Er 550 nm emission reaches 5× over the Ag-free structure. Also, the rapid transition between highly quenched and enhanced comes as a result of competition between the distance-dependent mechanisms.[13] Engineering the nanostructures to have a high Sca/Abs at the characteristic RE emission frequencies, with the optimal distance, is an important next step for applications using metal-enhanced UC. A high absorbance in the IR would be further beneficial for an enhanced excitation contribution.

As a preliminary study of the biocompability for bioimaging applications, we tested for cytotoxicity on prostate cell line PPC-1. We incubated the particles at various concentrations with the cells for ∼20 h and tested viability using the MTS assay. Despite the high concentrations and settling of particles onto the cell membranes (Figure 2D), the cells show high viability versus controls. To test the utility in imaging, while keeping in mind the oxide matrix is not the brightest UC material to begin with, two-photon images were collected after replacing the media. We could observe UC from bound particles under a femtosecond pulsed laser at 980 nm, using a scanning confocal system. Emission was collected from 550−600 nm (Figure S9). We are currently exploring surface coatings and pursuing more specific cell interactions and uptake studies as well as expanding the Ag enhancement to other UC materials.

In summary, the nanostructures that comprise silver cores and dense layers of Y_2O_3:Er separated by a silica shell are an excellent model system to study the interaction between upconversion materials and metals in nanoscale. This architecture allows for versatile control of the Y_2O_3:Er−metal interaction through control of the silica dielectric spacer thickness and the metal-core size. Finally, the nanoparticles are potentially interesting as fluorescent labels in, for instance (single particle), imaging experiments or bioassays which require low background or tissue penetrating wavelengths.

Acknowledgment. The authors acknowledge U.S. National Science Foundation (DMR 08-05148) and NSF of China (20721063, 20821140537). We thank Alexander Mikhailovsky for optical characterization.

Supporting Information Available: Experimental details, UV−vis−NIR spectra, and intensity time decay results. This material is available free of charge via the Internet at http://pubs.acs.org.

References

(1) Decher, G.; Schneider, G. *Nano Lett.* **2006**, *6*, 530.
(2) Liu, N.; Prall, B. S.; Klimov, V. *J. Am. Chem. Soc.* **2006**, *128*, 15362.
(3) Nabika, H.; Deki, S. *J. Phys. Chem. B* **2003**, *107*, 9161.
(4) West, J. L.; Halas, N. L. *Annu. Rev. Biomed. Eng.* **2003**, *5*, 285.
(5) Song, J. H.; Atay, T.; Shi, S.; Urabe, H.; Nurmikko, A. V. *Nano Lett.* **2005**, *5*, 1557.
(6) Wang, F.; Liu, X. G. *Chem. Soc. Rev.* **2009**, *38*, 976.
(7) Mertens, H.; Polman, A. *Appl. Phys. Lett.* **2006**, *89*, 211107.
(8) Karmakar, B; Som, T. *J. Appl. Phys.* **2009**, *105*, 013102.
(9) Sun, Y. G.; Xia, Y. N. *J. Am. Chem. Soc.* **2004**, *126*, 3892.
(10) Aiken, B.; Hsu, W. P.; Matijevic, E. *J. Am. Ceram. Soc.* **1988**, *71*, 845.
(11) Rai, V. K.; de Menezes, L. S; de Araujo, C. B.; Kassab, L. R. P.; da Silva, D. M.; Kobayashi, R. A. *J. Appl. Phys.* **2008**, *103*, 093526.
(12) Matsura, D.; Hattori, H.; Takano, A. *J. Electrochem. Soc.* **2005**, *152*, H39.
(13) Lakowicz, J. R. *Anal. Biochem.* **2005**, *337*, 171.

JA909108X